

1 An engineered decoy receptor for SARS-CoV-2 broadly binds 2 protein S sequence variants

3 Kui K. Chan¹, Timothy J.C. Tan², Krishna K. Narayanan² and Erik Procko²

4 ¹Orthogonal Biologics, Champaign IL 61821

5 ²Department of Biochemistry and Cancer Center at Illinois, University of Illinois, Urbana IL 61801

6 Correspondence: procko@illinois.edu

7 ABSTRACT

8 The spike S of SARS-CoV-2 recognizes ACE2 on the host cell membrane to initiate entry. Soluble decoy
9 receptors, in which the ACE2 ectodomain is engineered to block S with high affinity, potently neutralize
10 infection and, due to close similarity with the natural receptor, hold out the promise of being broadly
11 active against virus variants without opportunity for escape. Here, we directly test this hypothesis. We
12 find an engineered decoy receptor, sACE2_{v2.4}, tightly binds S of SARS-associated viruses from
13 humans and bats, despite the ACE2-binding surface being a region of high diversity. Saturation
14 mutagenesis of the receptor-binding domain followed by in vitro selection, with wild type ACE2 and the
15 engineered decoy competing for binding sites, failed to find S mutants that discriminate in favor of the
16 wild type receptor. We conclude that resistance to engineered decoys will be rare and that decoys may be
17 active against future outbreaks of SARS-associated betacoronaviruses.

18 INTRODUCTION

19 Zoonotic coronaviruses have crossed over from animal reservoirs multiple times in the past two
20 decades, and it is almost certain that wild animals will continue to be a source of devastating outbreaks.
21 Unlike ubiquitous human coronaviruses responsible for common respiratory illnesses, these zoonotic
22 coronaviruses with pandemic potential cause serious and complex diseases, in part due to their tissue
23 tropisms driven by receptor usage. Severe Acute Respiratory Syndrome Coronaviruses 1 (SARS-CoV-1)
24 and 2 (SARS-CoV-2) engage angiotensin-converting enzyme 2 (ACE2) for cell attachment and entry (*1-
25 7*). ACE2 is a protease responsible for regulating blood volume and pressure that is expressed on the
26 surface of cells in the lung, heart and gastrointestinal tract, among other tissues (*8, 9*). The ongoing spread
27 of SARS-CoV-2 and the disease it causes, COVID-19, has had a crippling toll on global healthcare
28 systems and economies, and effective treatments and vaccines are urgently needed.

29 As SARS-CoV-2 becomes endemic in the human population, it has the potential to mutate and
30 undergo genetic drift and recombination. To what extent this will occur as increasing numbers of people
31 are infected and mount counter immune responses is unknown, but already a variant in the viral spike
32 protein S (D614G) has rapidly emerged from multiple independent events and effects S protein stability
33 and dynamics (*10, 11*). Another S variant (D839Y) became prevalent in Portugal, possibly due to a
34 founder effect (*12*). Coronaviruses have moderate to high mutation rates. For example, 10^{-4} substitutions
35 per year per site occur in HCoV-NL63 (*13*), an alphacoronavirus that also binds ACE2, albeit via a
36 smaller interface that is only partially shared with the RBDs of SARS-associated betacoronaviruses (*14*).
37 Additionally, large changes in coronavirus genomes have frequently occurred in nature from
38 recombination events, especially in bats where co-infection levels can be high (*15, 16*). Recombination of
39 MERS-CoVs has also been documented in camels (*17*). This will all have profound implications for the
40 current pandemic's trajectory, the potential for future coronavirus pandemics, and whether drug resistance
41 in SARS-CoV-2 becomes prevalent.

42 The viral spike is a vulnerable target for neutralizing monoclonal antibodies that are progressing
43 through clinical trials, yet in tissue culture escape mutations in the spike rapidly emerge to all antibodies
44 tested (18). Deep mutagenesis of the isolated receptor-binding domain (RBD) by yeast surface display
45 has easily identified mutations in S that retain high expression and ACE2 affinity, yet are no longer bound
46 by monoclonal antibodies and confer resistance (19). This has motivated the development of cocktails of
47 non-competing monoclonals (18, 20), inspired by lessons learned from the treatment of HIV-1 and Ebola,
48 to limit the possibilities for the virus to escape. Notably, drug maker Eli Lilly has a monoclonal
49 monotherapy (LY-CoV555) in advanced trials (NCT04427501) where the emergence of resistant virus
50 variants has occurred; the trial has been updated to include an arm with a second monoclonal (LY-
51 CoV016). However, even the use of monoclonal cocktails does not address future coronavirus spill overs
52 from wild animals that may be antigenically distinct. Indeed, large screening efforts were required to find
53 antibodies from recovered SARS-CoV-1 patients that cross-react with SARS-CoV-2 (21), indicating
54 antibodies have confined capacity for interacting with variable epitopes on the spike surface, and are
55 unlikely to be broad and pan-specific for all SARS-related viruses.

56 An alternative protein-based antiviral to monoclonal antibodies is to use soluble ACE2 (sACE2) as a
57 decoy to compete for receptor-binding sites on the viral spike (6, 22-25). In principle, the virus has
58 limited potential to escape sACE2-mediated neutralization without simultaneously decreasing affinity for
59 the native ACE2 receptor, rendering the virus less virulent. Multiple groups have now engineered sACE2
60 to create high affinity decoys for SARS-CoV-2 that rival matured monoclonal antibodies and potently
61 neutralize infection (25-27). In our group, deep mutagenesis was used to identify a large number of
62 mutations in ACE2 that increase affinity for S (25). These mutations were dispersed across the interface
63 and also at distal sites where they are predicted to enhance folding of the virus-recognized conformation.
64 A combination of three mutations, called sACE2_{2.v2.4}, increases affinity 35-fold and binds SARS-CoV-2
65 S (K_D 600 pM) with affinity comparable to the best monoclonal antibodies (25). Even tighter apparent
66 affinities are reached through avid binding to trimeric spike expressed on a membrane. Despite
67 engineering being focused exclusively on SARS-CoV-2 affinity, sACE2_{2.v2.4} potently neutralized
68 authentic SARS-CoV-1 and -2 infection in tissue culture, suggesting it's close resemblance to the wild
69 type receptor confers broad activity against ACE2-utilizing betacoronaviruses generally. Soluble
70 ACE2_{2.v2.4} is dimeric and monodisperse without aggregation, catalytically active, highly soluble, stable
71 after storage at 37°C for days, and well expressed at levels greater than the wild type protein. Due to both
72 its high activity and favorable properties for manufacture, sACE2_{2.v2.4} is a genuine drug candidate for
73 preclinical development.

74 Engineered, high affinity decoy receptors, while very similar to natural ACE2, nonetheless have
75 mutations present at or near the interaction surface. There is therefore an opportunity for viral spike
76 variants to discriminate between an engineered decoy and wild type receptors, providing a route towards
77 resistance. Here, we show that the engineered decoy sACE2_{2.v2.4} binds broadly and tightly to the RBDs
78 of diverse SARS-associated betacoronaviruses that use ACE2 for entry. We further fail to find mutations
79 within the RBD, which directly contacts ACE2 and is where possible escape mutations will most likely
80 reside, that redirect specificity towards the wild type receptor. We conclude that resistance to an
81 engineered decoy receptor will be rare, and sACE2_{2.v2.4} targets common attributes for affinity to S in
82 SARS-associated viruses.

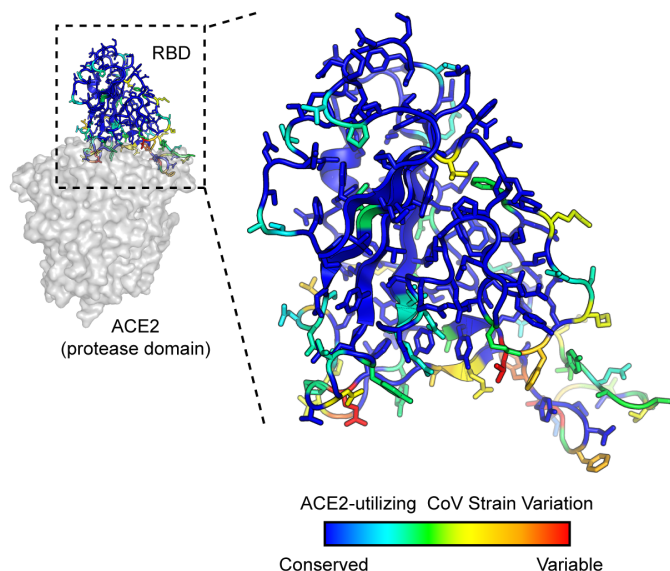
83 RESULTS

84 An engineered decoy receptor broadly binds RBDs from SARS-associated CoVs with tight affinity

85 The affinities of the decoy receptor sACE2_{2.v2.4} were determined for purified RBDs from the S
86 proteins of five coronaviruses from *Rhinolophus* bat species (isolates LYRa11, Rs4231, Rs7327, Rs4084
87 and RsSHC014) and two human coronaviruses, SARS-CoV-1 and SARS-CoV-2. These viruses fall

88 within a common clade of betacoronaviruses that use ACE2 as an entry receptor (7). They share close
 89 sequence identity within the RBD core while variation is highest within the functional ACE2 binding site
 90 (Figures 1 and S1), possibly due to a co-evolutionary 'arms race' with polymorphic ACE2 sequences in
 91 ecologically diverse bat species (28). Affinity was measured by biolayer interferometry (BLI), with
 92 sACE2₂ (a.a. S19-G732) fused at the C-terminus with the Fc moiety of human IgG1 immobilized to the
 93 sensor surface and monomeric 8his-tagged RBD (Figure S2) used as the soluble analyte. This
 94 arrangement excludes avidity effects, which otherwise cause artificially tight (picomolar) apparent
 95 affinities whenever dimeric sACE2₂ in solution is bound to immobilized RBD decorating an interaction
 96 surface. Wild type sACE2₂ bound all the RBDs with affinities ranging from 16 nM for SARS-CoV-2 to
 97 91 nM for LYRa11, with median affinity 60 nM (Table 1). The measured affinities for the RBDs of
 98 SARS-CoV-1 and SARS-CoV-2 are comparable to published data (4, 25, 29-31). Engineered
 99 sACE2₂.v2.4 displayed large increases in affinity for all the RBDs, with K_Ds ranging from 0.4 nM for
 100 SARS-CoV-2 to 3.5 nM for isolate Rs4231, with median affinity less than 2 nM (Table 1). The
 101 approximate 35-fold affinity increase of the engineered decoy applies universally to coronaviruses in the
 102 test panel and the molecular basis for affinity enhancement must therefore be grounded in common
 103 attributes of RBD/ACE2 recognition.

104 **Figure 1. SARS-associated coronaviruses have high sequence diversity at the ACE2-binding site.**
 105 The RBD of SARS-CoV-2 (PDB 6M17) is colored by diversity between 7 SARS-associated CoV strains
 106 (blue, conserved; red, variable).



107

108

Table 1. BLI kinetics for immobilized sACE2 ₂ -IgG1 binding to coronavirus RBDs								
CoV strain ^a	Wild type sACE2 ₂ -IgG1 ^b				sACE2 ₂ .v2.4-IgG1			
	k _{on} (M ⁻¹ s ⁻¹)	k _{off} (s ⁻¹)	K _D (nM)	χ ² ^c	k _{on} (M ⁻¹ s ⁻¹)	k _{off} (s ⁻¹)	K _D (nM)	χ ²
LYRa11	8.7 × 10 ⁵	7.9 × 10 ⁻²	91	0.12	1.4 × 10 ⁶	2.5 × 10 ⁻³	1.8	0.10
Rs7327	6.4 × 10 ⁵	4.0 × 10 ⁻²	63	0.25	9.8 × 10 ⁵	1.8 × 10 ⁻³	1.9	0.11
Rs4231	3.2 × 10 ⁵	2.2 × 10 ⁻²	69	0.04	4.5 × 10 ⁵	1.6 × 10 ⁻³	3.5	0.10
Rs4084	2.9 × 10 ⁵	2.5 × 10 ⁻²	85	0.24	4.8 × 10 ⁵	1.5 × 10 ⁻³	3.1	0.10
RsSHC014	8.8 × 10 ⁵	2.6 × 10 ⁻²	29	0.20	1.6 × 10 ⁶	2.0 × 10 ⁻³	1.3	0.29

SARS-1	6.6×10^3	1.2×10^{-4}	58	0.03	3.0×10^3	5.6×10^{-6}	2.1	0.03
SARS-2	1.4×10^6	8.1×10^{-3}	16	0.25	6.6×10^5	2.8×10^{-4}	0.4	0.09

^a Purified RBDs at 5 to 7 concentrations were used as the soluble analytes.

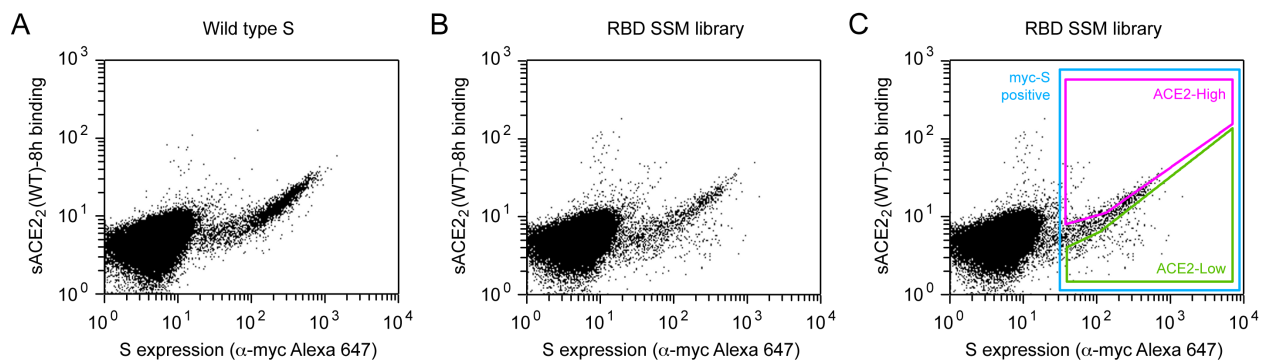
^b IgG1-Fc fused sACE2₂ was immobilized to anti-human IgG Fc capture biosensors.

^c χ^2 values represent the goodness of curve fitting. Acceptable values were considered to be less than 3.

109
110 **A deep mutational scan of the RBD in the context of full-length S reveals residues in the ACE2**
111 **binding site are mutationally tolerant**

112 To explore potential sequence diversity in S of SARS-CoV-2 that may act as a 'reservoir' for drug
113 resistance, the mutational tolerance of the RBD was evaluated by deep mutagenesis (32). Saturation
114 mutagenesis was focused to the RBD (a.a. C336-L517) of full-length S tagged at the extracellular N-
115 terminus with a c-myc epitope for detection of surface expression. The spike library, encompassing 3,640
116 single amino acid substitutions, was transfected in human Expi293F cells under conditions where cells
117 typically acquire no more than a single sequence variant (33, 34). The culture was incubated with wild
118 type, 8his-tagged, dimeric sACE2₂ at a sub-saturating concentration (2.5 nM). Bound sACE2₂-8h and
119 surface-expressed S were stained with fluorescent antibodies for flow cytometry analysis (Figure 2A).
120 Compared to cells expressing wild type S, the library was poorly expressed, indicating many mutations
121 are deleterious for folding and expression. A cell population was clearly discernable expressing S
122 variants that bind ACE2 with decreased affinity (Figure 2B). After gating for c-myc-positive cells
123 expressing S, cells with high and low levels of bound sACE2₂ were collected by fluorescence-activated
124 cell sorting (FACS), called the ACE2-High and ACE2-Low populations, respectively (Figure 2C). Both
125 the expression and sACE2₂ binding signals decreased over minutes to hours during sorting, possibly due
126 to shedding of the S1 subunit. Cells were therefore collected and pooled from three separate FACS
127 experiments for a combined 8 hours sort time.

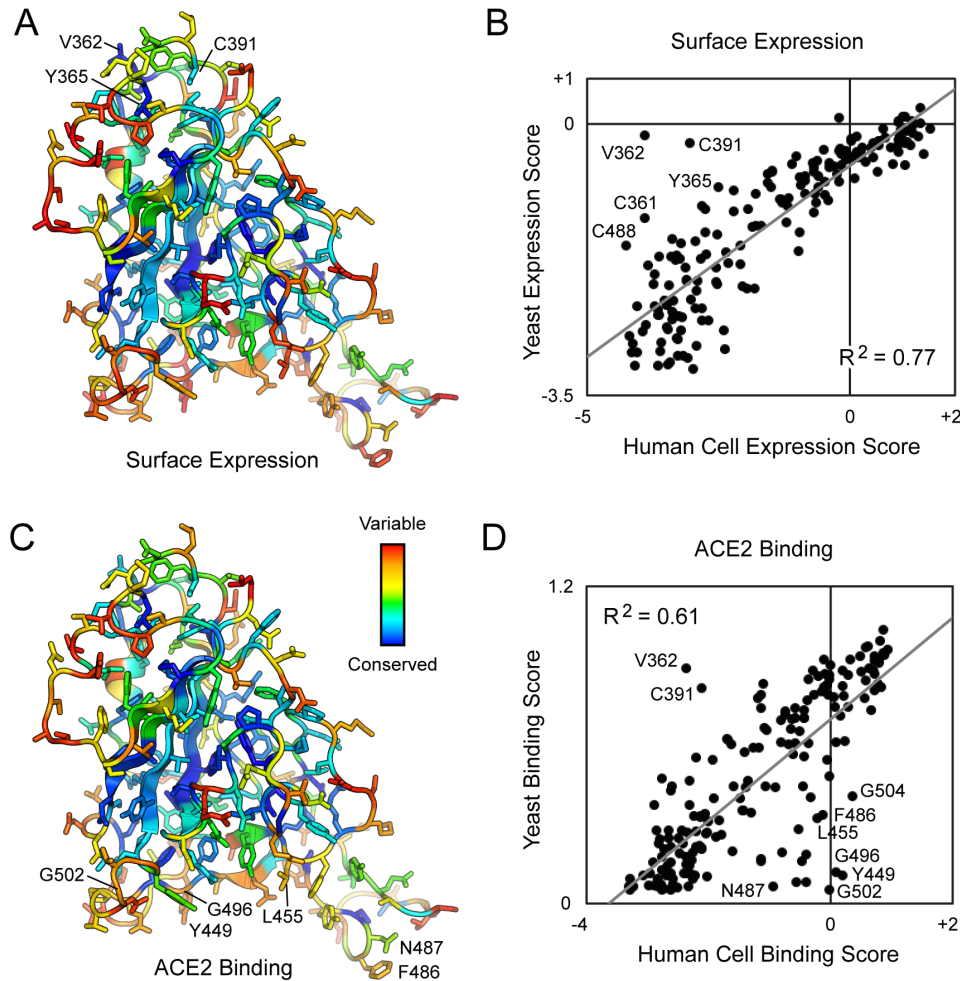
128 **Figure 2. FACS selection for variants of S with high or low binding signal to ACE2. (A)** Flow
129 cytometry analysis of Expi293F cells expressing full-length S of SARS-CoV-2 with an N-terminal c-myc
130 tag. Staining for the myc-epitope is on the x-axis while the detection of bound sACE2₂-8h (2.5 nM) is on
131 the y-axis. S plasmid was diluted 1500-fold by weight with carrier DNA so that cells typically express no
132 more than one coding variant; under these conditions most cells are negative. **(B)** Flow cytometry of cells
133 transfected with the RBD single site-saturation mutagenesis (SSM) library shows cells expressing S
134 variants with reduced sACE2₂-8h binding. **(C)** Gating strategy for FACS. S-expressing cells positive for
135 the c-myc epitope were gated (blue) and the highest ("ACE2-High") and lowest ("ACE2-Low") 20% of
136 cells with bound sACE2₂-8h relative to myc-S expression were collected.



137
138 Transcripts in the sorted cells were Illumina sequenced and compared to the naive plasmid library to
139 determine an enrichment ratio for each amino acid substitution (35). Mutations in S that express and bind
140 ACE2 tightly are selectively enriched in the ACE2-High sort (Figure S3); mutations that express but have
141 reduced ACE2 binding are selectively enriched in the ACE2-Low sort; and mutations that are poorly

142 expressed are depleted from both sorted populations. Positional conservation scores were calculated by
143 averaging the \log_2 enrichment ratios for each of the possible amino acids at a residue position. By adding
144 conservation scores for both the ACE2-High and ACE2-Low sorts we derive a score for surface
145 expression, which shows that the hydrophobic RBD core is tightly conserved for folding and trafficking
146 of the viral spike (Figure 3A). By comparison, residues on the exposed RBD surface are mutationally
147 permissive for S surface expression. This matches the mutational tolerance of proteins generally.

148 **Figure 3. Deep mutagenesis reveals that the ACE2-binding site of SARS-CoV-2 tolerates many**
149 **mutations. (A)** Positional scores for surface expression are mapped to the structure of the SARS-CoV-2
150 RBD (PDB 6M17, oriented as in Figure 1). Blue residues in the protein core are highly conserved in the
151 FACS selection for surface S expression (judged by depletion of mutations from the ACE2-High and
152 ACE2-Low gates), while surface residues in red tolerate mutations. **(B)** Correlation plot of expression
153 scores from mutant selection in human cells of full-length S (x-axis) versus the conservation scores
154 (mean of the \log_2 enrichment ratios at a residue position) from mutant selection in the isolated RBD by
155 yeast display (y-axis). Notable outliers are indicated. **(C)** Conservation scores from the ACE2-High gated
156 cell population are mapped to the RBD structure, with residues colored from low (blue) to high (red)
157 mutational tolerance. **(D)** Correlation plot of RBD conservation scores for high ACE2 binding from deep
158 mutagenesis of S in human cells (x-axis) versus deep mutagenesis of the RBD on the yeast surface
159 (mean of $\Delta K_{D\text{ app}}$; y-axis).



161 For tight ACE2 binding (i.e. S variants in the ACE2-High population), conservation increases for
162 RBD residues at the ACE2 interface, yet mutational tolerance remains high (Figure 3C). The sequence
163 diversity observed among natural betacoronaviruses, which display high diversity at the ACE2 binding
164 site, is therefore replicated in the deep mutational scan, which predicts the SARS-CoV-2 spike tolerates
165 substantial genetic diversity at the receptor-binding site for function. From this accessible sequence
166 diversity SARS-CoV-2 might feasibly mutate to acquire resistance to monoclonal antibodies or
167 engineered decoy receptors targeting the ACE2-binding site.

168 **Comparison to a deep mutational scan of the isolated RBD by yeast surface display**

169 Two deep mutational scans have been reported for the isolated RBD displayed on the surface of
170 yeast (36, 37). We compare our data, from a selection of full-length S expressed in human cells, to the
171 publicly accessible Starr et al data set (36). Important residues within the RBD for surface expression of
172 full-length spike in human cells are closely correlated with data from yeast surface display of the isolated
173 RBD (Figure 3B), with the exception of a notable region. The surface of the RBD opposing the ACE2-
174 binding site (e.g. V362, Y365 and C391) is free to mutate for yeast surface display, but its sequence is
175 constrained in our experiments; this region of the RBD is buried by connecting structural elements to the
176 global fold of an S subunit in the closed-down conformation (this is the dominant conformation for S
177 subunits and is inaccessible to receptor binding) (2, 4, 38, 39). We used targeted mutagenesis to
178 individually test alanine substitutions to all the cysteines in the RBD (Figure S4). We found all cysteine-
179 to-alanine mutations severely diminish S surface expression in Expi293F cells, including C391A and
180 C525A on the RBD 'backside' that were neutral in the yeast display scan (36). These differences
181 demonstrate that there are tighter sequence constraints on the RBD in the context of a full spike expressed
182 at a human cell membrane, yet overall we consider the two data sets to closely agree.

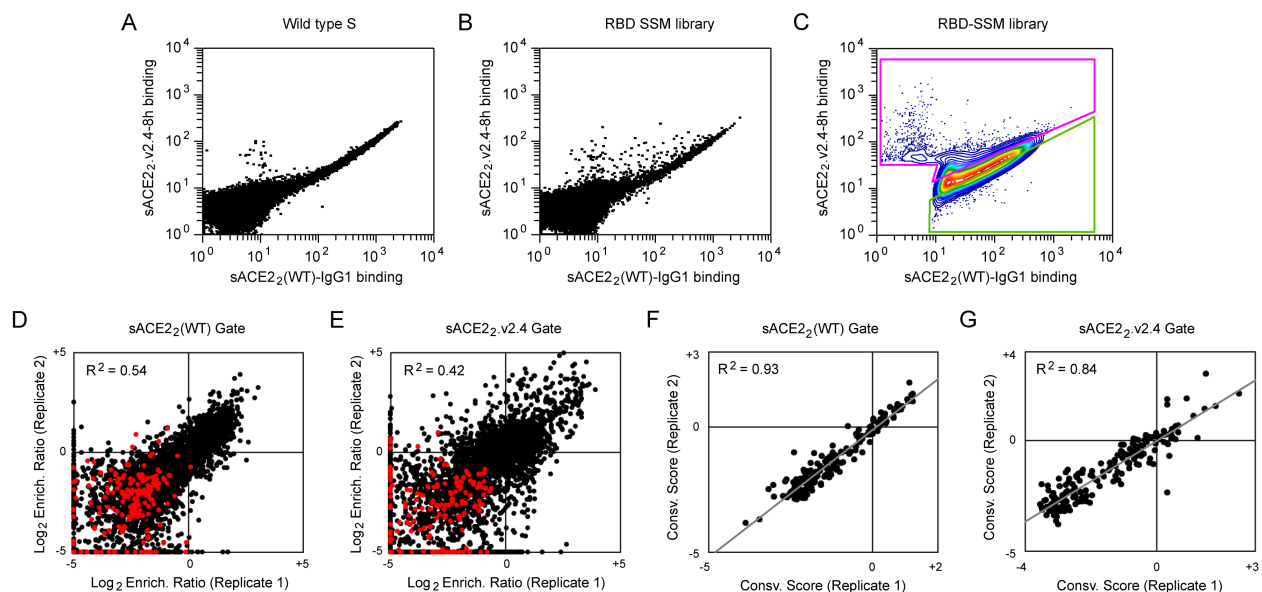
183 For binding to dimeric sACE2₂, we note that interface residues were more tightly conserved in the
184 Starr et al data set (Figure 3D), possibly a consequence of three differences between the deep mutagenesis
185 experiments. First, our selections for ACE2 binding of S variants at the plasma membrane appears to
186 primarily reflect mutational effects on surface expression, which is almost certainly more stringent in
187 human cells. Yeast permit many poorly folded proteins to leak to the cell surface (40). Second, the yeast
188 selections were conducted at multiple sACE2 concentrations from which apparent K_D changes were
189 computed (36); the Starr et al data in this regard is very comprehensive. Due to the long sort times
190 required for our human cell libraries where only a small fraction of cells express spike, we sorted at a
191 single sACE2₂ concentration that cannot accurately capture a range of different binding affinities
192 quantitatively. Third, dimeric sACE2₂ may geometrically complement trimeric S densely packed on a
193 human cell membrane, such that avidity masks the effects of affinity-reducing mutations. Nonetheless,
194 there is overall agreement that ACE2 binding often persists following mutations to the RBD surface, and
195 our data simply suggests mutational tolerance may be even greater than that already observed by Starr et
196 al.

197 **A screen for S variants that preferentially bind wild type ACE2 over the engineered decoy**

198 Having shown that the ACE2-binding site of SARS-CoV-2 protein S tolerates many mutations, we
199 asked whether mutations might therefore be found that confer resistance to the engineered decoy
200 sACE2₂.v2.4. Resistance mutations are anticipated to lose affinity for sACE2₂.v2.4 while maintaining
201 binding to the wild type receptor, and are most likely to reside in the RBD where physical contacts are
202 made. Similar reasoning formed the foundation of a deep mutagenesis-based selection of the isolated
203 RBD by yeast surface display to find escape mutations to monoclonal antibodies, and the results were
204 predictive of escape mutations in pseudovirus growth selections (19).

205 To address whether escape mutations from the engineered decoy might be found in the RBD, we
206 repurposed the S protein library for a specificity selection. Cells expressing the library, encoding all
207 possible substitutions in the RBD, were co-incubated with wild type sACE2₂ fused to the Fc region of
208 IgG1 and 8his-tagged sACE2₂.v2.4 at concentrations where both proteins bind competitively (25). It was
209 immediately apparent from flow cytometry of the Expi293F culture expressing the S library that there
210 were cells expressing S variants shifted towards preferential binding to sACE2₂.v2.4, but no significant
211 population with preferential binding to the wild type receptor (Figures 4A and 4B). Cells expressing S
212 variants that might preferentially bind sACE2₂(WT)-IgG1 or sACE2₂.v2.4 were gated and collected by
213 FACS (Figure 4C), followed by deep sequencing of S transcripts to determine enrichment ratios. There
214 was close agreement between two independent replicate experiments (Figures 4D-4G). Most RBD
215 mutations were depleted following sorting, consistent with deleterious effects on S folding and
216 expression.

217 **Figure 4. A competition-based selection to identify RBD mutations within S of SARS-CoV-2 that**
218 **preferentially bind wild type or engineered ACE2 receptors. (A)** Expi293F cells were transfected with
219 wild type myc-S and incubated with competing sACE2₂(WT)-IgG1 (25 nM) and sACE2₂.v2.4-8h (20 nM).
220 Bound protein was detected by flow cytometry after immuno-staining for the respective epitope tags. **(B)**
221 As in A, except cells were transfected with the RBD SSM library. A population of cells expressing S
222 variants with increased specificity towards sACE2₂.v2.4 is apparent (cells shifted to the upper-left of the
223 main population). **(C)** Gates used for FACS of cells expressing the RBD SSM library. After excluding
224 cells without bound protein, the top 20% of cells for bound sACE2₂.v2.4-8h (magenta gate) and for bound
225 sACE2₂(WT)-IgG1 (green gate) were collected. **(D-E)** Agreement between log₂ enrichment ratios from two
226 independent FACS selections for cells expressing S variants with increased specificity for (D)
227 sACE2₂(WT) or (E) sACE2₂.v2.4. R² values are calculated for nonsynonymous mutations (black).
228 Nonsense mutations are red. **(F-G)** Conservation scores are calculated from the mean of the log₂
229 enrichment ratios for all nonsynonymous substitutions at a given residue position. Correlation plots show
230 agreement between conservation scores for two independent selections for cells within the (D)
231 sACE2₂(WT) or (E) sACE2₂.v2.4 specific gates.

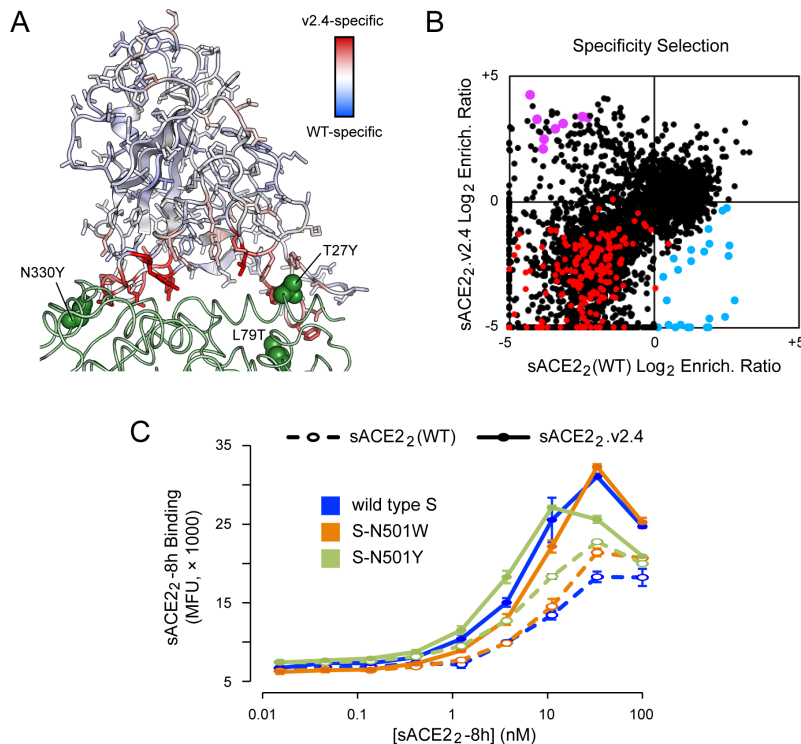


232

233 Soluble ACE2₂.v2.4 has three mutations from wild type ACE2: T27Y buried within the RBD
234 interface, and L79T and N330Y at the interface periphery (Figure 5A). A substantial number of mutations
235 in the RBD of S were selectively enriched for preferential binding to sACE2₂.v2.4 (Figure 5B, upper-left
236 quadrant). While sACE2₂.v2.4-specificity mutations could be found immediately adjacent to the sites of
237 engineered mutations in ACE2 (in particular mutations to S-F486 adjacent to ACE2-L79 and S-T500

238 adjacent to ACE2-N330), major hot spots for sACE2₂.v2.4-specificity mutations were also mapped to
239 RBD loop 498-506, contacting the region where the ACE2- α 1 helix packs against a β -hairpin motif
240 (Figure 5A). By comparison, there were no hot spots in the RBD for sACE2₂(WT)-specificity mutations.
241 Indeed, only a small number of mutations were selectively enriched for preferential binding to wild type
242 receptor (Figure 5B), and the abundance of these putative wild type-specific mutations barely rose above
243 the expected level of noise in the deep mutagenesis data. In this competition assay, S binding to wild type
244 sACE2₂ is therefore more sensitive to RBD mutations than S binding to engineered sACE2₂.v2.4.

245 **Figure 5. Mutations within the RBD that confer specificity towards wild type ACE2 are rare. (A)** The
246 SARS-CoV-2 RBD is colored by specificity score (the difference between the conservation scores for cells
247 collected in the sACE2₂(WT) and sACE2₂.v2.4 specific gates). Residues that are hot spots for mutations
248 with increased specificity towards sACE2₂(WT) are blue or towards sACE2₂.v2.4 are red. The contacting
249 surface of ACE2 is shown as a green ribbon, with sites of mutations in sACE2₂.v2.4 labeled and shown
250 as green spheres. **(B)** Log₂ enrichment ratios for mutations in S expressed by cell populations collected in
251 the sACE2₂(WT) (x-axis) and sACE2₂.v2.4 (y-axis) specific gates. Data are the mean from two
252 independent sorting experiments. S mutants in blue were predicted to have increased specificity for
253 sACE2₂(WT) and were tested by targeted mutagenesis in Figure S5. S mutants in purple were predicted
254 to have increased specificity for sACE2₂.v2.4 and were tested by targeted mutagenesis in Figure S6.
255 Other nonsynonymous mutations are black. Nonsense mutations are red. **(C)** Wild type myc-S (blue) and
256 two variants, N501W (orange) and N501Y (green), were expressed in Expi293F cells and tested by flow
257 cytometry for binding to sACE2₂(WT)-8h (dashed lines) or sACE2₂.v2.4-8h (solid lines). Minor increases
258 in specific binding for wild type sACE2₂ are observed.



259

260 To determine whether the potential wild type ACE2-specific mutations found by deep mutagenesis
261 are real as opposed to false predictions due to data noise, we tested 24 mutants of S selectively enriched in
262 the wild type-specific gate by targeted mutagenesis (blue data points in Figure 5B). Only minor shifts
263 towards binding wild type sACE2₂ were observed (Figure S5). Two S mutants were investigated further
264 in sACE2₂ titration experiments, N501W and N501Y, which both retained high receptor binding and
265 displayed small shifts towards wild type sACE2₂ in the competition experiment. N501 of S is located in

266 the 498-506 loop and its substitution to large aromatic side chains might alter the loop conformation to
267 cause steric strain with nearby ACE2 mutation N330Y in sACE2₂.v2.4. After titrating the concentrations
268 of 8his-tagged sACE2₂(WT) and sACE2₂.v2.4 and measuring bound protein to S-expressing cells by flow
269 cytometry, it was found S-N501W and S-N501Y do show enhanced specificity for wild type sACE2₂, but
270 the effect is small and sACE2₂.v2.4 remains the stronger binder (Figure 5C); these mutations therefore
271 will not confer resistance in the virus to the engineered decoy. By comparison, multiple independent
272 escape mutations are readily found in S of SARS-CoV-2 that diminish the efficacy of monoclonal
273 antibodies by many orders of magnitude (18, 19).

274 Finally, 8 representative mutations to S predicted from the deep mutational scan to increase
275 specificity towards sACE2₂.v2.4 (purple data points in Figure 5B) were cloned and 7 were found to have
276 large shifts towards preferential sACE2₂.v2.4 binding in the competition assay (Figure S6). These S
277 mutations were Y449K/Q/S, L455G/R/Y and G504K. None of the mutated sites is in direct contact with
278 an engineered residue on sACE2₂.v2.4 and the molecular bases for specificity changes are therefore
279 ambiguous, but we speculate may involve local conformational perturbations. Validation by targeted
280 mutagenesis therefore confirms that the selection can successfully find mutations in S with altered
281 specificity. The inability to find mutations in the RBD that impart high specificity for the wild type
282 receptor means such mutations are rare or may not even exist, at least within the receptor-binding domain
283 where direct physical contacts with receptors occur. We cannot exclude mutations elsewhere having
284 long-range conformational effects. Engineered, soluble decoy receptors therefore live up to their promise
285 as broad therapeutic candidates against which a virus cannot easily escape.

286 DISCUSSION

287 The allure of soluble decoy receptors is that the virus cannot easily mutate to escape neutralization.
288 Mutations that reduce affinity of the soluble decoy will likely also decrease affinity for the wild type
289 receptor on host cells, thereby coming at the cost of diminished infectivity and virulence. However, this
290 hypothesis has not been rigorously tested, and since engineered decoy receptors differ from their wild
291 type counterparts, even if by just a small number of mutations, it is possible a virus may evolve to
292 discriminate between the two. Here, we show that an engineered decoy receptor for SARS-CoV-2
293 broadly binds with low nanomolar K_D to the spikes of SARS-associated betacoronaviruses that use ACE2
294 for entry, despite high sequence diversity within the ACE2-binding site. Mutations in S of SARS-CoV-2
295 that confer high specificity for wild type ACE2 were not found in a comprehensive screen of all
296 substitutions within the RBD. The engineered decoy receptor is therefore broad against zoonotic ACE2-
297 utilizing coronaviruses that may spill over from animal reservoirs in the future and against variants of
298 SARS-CoV-2 that may arise as the current COVID-19 pandemic rages on. We argue it is unlikely that
299 decoy receptors will need to be combined in cocktail formulations, as is required for monoclonal
300 antibodies or designed miniprotein binders to prevent the rapid emergence of resistance (18, 41),
301 facilitating manufacture and distribution. Our findings give insight into how a potential therapeutic can
302 achieve breath with a low chance of virus resistance for a family of highly infectious and deadly viruses.

303 Soluble decoy receptors have proven effective in the clinic, especially for modulating immune
304 responses. Etanercept (trade name Enbrel; soluble TNF receptor), aflibercept (Eylea; a soluble chimera of
305 VEGF receptors 1 and 2) and abatacept (Orencia; soluble CTLA-4) are just three examples of soluble
306 receptors that have profoundly impacted the treatment of human disease (42), yet no soluble receptors for
307 a viral pathogen are approved drugs. There are two main reasons for this. First, the affinity of entry
308 receptors for viral glycoproteins is often moderate to low, which reduces neutralization potency compared
309 to affinity-matured monoclonal antibodies. For SARS-CoV-2, we and others have solved this problem by
310 engineering ACE2 to have picomolar affinity for viral S (25-27). Second, virus entry receptors have
311 endogenous functions for normal physiology and their soluble counterparts may impact this normal
312 physiology to exert unacceptable toxicity. For example, the entry receptor for human cytomegalovirus is

313 a growth factor receptor, and growth factor interactions had to be knocked out to make a virus-specific
314 decoy suitable for in vivo administration (43). However, ACE2 in this regard is different and its
315 endogenous activity – the catalytic conversion of vasoconstrictive and inflammatory peptides of the renin-
316 angiotensin system – may be of direct benefit for addressing COVID-19 symptoms. During infection,
317 ACE2 activity is dysregulated and the renin-angiotensin system becomes imbalanced, possibly driving
318 aspects of acute-respiratory distress syndrome (ARDS) (44-46). Administration of recombinant sACE2
319 converts angiotensin (Ang) I and II to the protective peptides Ang-(1-9) and Ang-(1-7), respectively, with
320 potential benefits for the pulmonary and cardiovascular systems that include decreased lung elastance,
321 increased blood oxygenation, reduced hypertension and diminished inflammation (44, 45, 47-50).
322 Soluble, wild type ACE₂ has been developed as a drug for ARDS with an acceptable safety profile in
323 humans (51, 52) and is currently under evaluation in a clinical trial by Apeiron. Promisingly, a first
324 clinical case report found that administration of wild type sACE₂ was correlated with reduced viral
325 burden and improved clinical outcomes in a 45 year old woman with severe COVID-19
326 (DOI:[https://doi.org/10.1016/S2213-2600\(20\)30418-5](https://doi.org/10.1016/S2213-2600(20)30418-5)). Engineered, high affinity sACE₂ decoys, most
327 likely as fusions with immunoglobulin Fc for increased serum stability (23, 50, 53), represent next
328 generation therapeutics with dual mechanisms of action: (i) potent virus neutralization due to high affinity
329 blockade of the viral spike and (ii) proteolytic turnover of peptide hormones for direct relief of COVID-
330 19 symptoms.

331 MATERIALS AND METHODS

332 **Plasmids.** Residue numbers for constructs begin from the start methionine as amino acid (a.a.) 1. The
333 cloning of human codon-optimized, mature S from SARS-CoV-2 (GenBank Acc. No. YP_009724390.1;
334 a.a. V16-T1273) into the NheI-XhoI sites of pCEP4 (Invitrogen) with an N-terminal, extracellular c-myc
335 tag is described elsewhere (25). Soluble ACE2 (a.a. 1-732 encoding a dimer; wild type or engineered
336 variant sACE₂.v2.4) fused to an 8his purification tag or to human IgG1-Fc (a.a. D221-K447; nG1m1
337 isoallotype; GenBank KY432415.1) and cloned in to the NheI-XhoI sites of pcDNA3.1(+) (Invitrogen) is
338 also previously described (25). The RBDs of SARS-CoV-1 (Urbani isolate; GenBank AAP13441.1; a.a.
339 T320-D518), SARS-CoV-2 (YP_009724390; a.a. T333-K529), LYRa11 (AHX37558.1; a.a. T324-D522),
340 Rs7327 (ATO98218.1; a.a. T321-D519), Rs4231 (ATO98157.1; a.a. T320-D518), Rs4084 (ATO98132.1;
341 a.a. T321-D519) and RsSHC014 (AGZ48806.1; a.a. T321-D519) were cloned with N-terminal influenza
342 HA leader peptides (sequence MKTIIALSYIFCLVFA) and C-terminal 8-his tags (sequence
343 GSGHHHHHHHH) into the NheI-XhoI sites of pcDNA3.1(+). These plasmids are deposited with
344 Addgene under accession numbers 145145 and 161821-161826. Mutations were made by overlap
345 extension PCR and verified by Sanger sequencing.

346 **Tissue Culture.** Expi293F cells (ThermoFisher) were grown in Expi293 Expression Medium
347 (ThermoFisher) at 125 rpm, 8 % CO₂, 37 °C.

348 **Recombinant Protein Production.** Plasmids (500 ng DNA per ml culture) and polyethylenimine (MW
349 25,000; Polysciences; 3 µg per ml culture) were mixed with OptiMEM (Gibco; 100 µl per ml culture),
350 incubated 20 minutes at room temperature and added to Expi293F cells at a density of 2×10^6 / ml.
351 Transfection Enhancers (ThermoFisher) were added 18-23 h post-transfection. Culture supernatant was
352 harvested 4-6 days later by two centrifugation steps (800 × g for 10 minutes to remove cells and 20,000 ×
353 g for 20 minutes to remove debris). IgG1 Fc fused and 8his-tagged proteins were subsequently purified as
354 previously described (25) using KANEKA KanCapA 3G Affinity (Pall) and HisPur Ni-NTA (Thermo
355 Scientific) resins, respectively. Eluted proteins from affinity chromatography were then separated on a
356 Superdex 200 Increase 10/300 GL column (GE Healthcare Life Sciences) equilibrated with Dulbecco's
357 phosphate-buffered saline (PBS). Proteins from peak fractions were concentrated using centrifugal
358 ultrafiltration devices (Millipore) to final concentrations of ~1 mg/ml (RBD-8h proteins), ~10 mg/ml
359 (sACE₂-8h proteins) and ~50 mg/ml (sACE₂-IgG1 proteins). Concentrations were determined by

360 absorbance at 280 nm using calculated extinction coefficients. Reported concentrations for sACE₂ are
361 based on monomeric subunits. Aliquots were snap frozen in liquid N₂ and stored at -80 °C.

362 **Biolayer Interferometry.** BLI kinetics were collected on an Octet RED96a and analyzed with a 1:1
363 binding model (global fit) using instrument software (Molecular Devices). IgG1 Fc-fused sACE₂ (wild
364 type or engineered variant sACE₂.v2.4) were immobilized at 100 nM for 10 minutes to anti-human IgG
365 Fc biosensors (Molecular Devices). The assay buffer was 10 mM HEPES pH 7.6, 150 mM NaCl, 3 mM
366 EDTA, 0.05% polysorbate 20, 0.5% non-fat dry milk (Bio-Rad). Loaded sensors were equilibrated for 30
367 s in buffer, then dipped in RBD-8h solutions for 60 s to measure association and transferred back to
368 buffer to measure dissociation over 300 s.

369 **Library Construction, FACS and Illumina Sequencing Analysis.** Using plasmid pCEP4-myc-S
370 encoding tagged, full length S of SARS-CoV-2, saturation mutagenesis was focused to residues C336-
371 L517 forming the RBD. Degenerate NNK codons were introduced at all RBD positions using overlap
372 extension PCR as previously described (54). Transient transfection conditions were used that typically
373 provide no more than a single coding variant per cell (33, 34). Expi293F cells at 2×10^6 / ml were
374 transfected with a mixture of 1 ng coding plasmid (i.e. library DNA) with 1.5 µg pCEP4-ΔCMV carrier
375 plasmid (described in (34)). The medium was replaced 2 h post-transfection and cells were collected 24 h
376 post-transfection for FACS. Cells were washed with ice-cold PBS supplemented with 0.2 % bovine serum
377 albumin (PBS-BSA).

378 For investigations of binding to wild type sACE₂, the cells expressing the S library were resuspended in
379 2.5 nM sACE₂(WT)-8h and incubated 30 minutes on ice. Cells were washed twice with PBS-BSA and
380 then co-stained for 20 minutes with anti-myc Alexa 647 (clone 9B11, 1/250 dilution; Cell Signaling
381 Technology) and anti-HIS-FITC (chicken polyclonal, 1/100 dilution; Immunology Consultants
382 Laboratory). Cells were again washed twice before sorting on a BD FACS Aria II at the Roy J. Carver
383 Biotechnology Center. Dead cells, doublets and debris were excluded by first gating on the main
384 population by forward/side scattering and then excluding DAPI positive cells. From the myc-S-positive
385 (Alexa 647) population, the 20 % of cells with the highest and 20% of cells with the lowest anti-HIS-
386 FITC fluorescence for bound sACE₂(WT)-8h were collected (Figure 2C). Collection tubes were coated
387 overnight with fetal bovine serum prior to sorting and contained Expi293 Expression Medium. Collected
388 cell pellets were frozen at -80°C and were pooled across separate sort experiments prior to extraction of
389 total RNA.

390 The competition selection was performed similarly, with the exception that cells expressing the S library
391 were incubated for 30 minutes in a mixture of 20 nM sACE₂.v2.4-8h and 25 nM sACE₂(WT)-IgG1.
392 After washing twice, bound proteins were stained for 30 minutes with anti-human IgG-APC (clone
393 HP6017, 1/250 dilution; BioLegend) and anti-HIS-FITC (chicken polyclonal, 1/100 dilution;
394 Immunology Consultants Laboratory). Cells were washed twice and sorted. After gating for the main
395 population of viable cells as described above, the 20 % of cells with the highest FITC-relative-to-APC
396 and highest APC-relative-to-FITC signals were collected (Figure 4C).

397 Total RNA was extracted from the collected cells using a GeneJET RNA purification kit (Thermo
398 Scientific). First strand cDNA was synthesized with Accuscript (Agilent) primed with a gene-specific
399 oligonucleotide. The region of S scanned by saturation mutagenesis was PCR amplified as 3 overlapping
400 fragments that together span the full RBD sequence. Following a second round of PCR, primers added
401 adapters for annealing to the Illumina flow cell and sequencing primers, together with barcodes for
402 experiment identification. The PCR products were sequenced on an Illumina NovaSeq 6000 using a
403 2×250 nt paired end protocol. Data were analyzed using Enrich (35), where the frequencies of S variants
404 in the transcripts of the sorted populations were compared to their frequencies in the naive plasmid
405 library. Log₂ enrichment ratios for all the individual mutations were calculated and normalized by

406 subtracting the log₂ enrichment ratio for the wild type sequence across the same PCR-amplified fragment.
407 Conservation scores at residue positions were calculated by averaging the log₂ enrichment ratios for all
408 non-synonymous mutations at the residue.

409 **Flow Cytometry Analysis of SARS-CoV-2 S Mutants.** Expi293F cells at 2.0×10^6 cells/ml were
410 transfected with plasmid DNA (300 ng per ml of culture for measuring myc-S surface expression and
411 sACE2₂ competition binding, 500 ng per ml for titration experiments) encoding myc-S variants using
412 Expifectamine (ThermoFisher) according to the manufacturer's directions. At 24 h post-transfection, cells
413 were washed with PBS-BSA. To detect surface expressed myc-S, cells were incubated with anti-myc
414 Alexa 647 (clone 9B11, 1/250 dilution; Cell Signaling Technology) on a rocker at 4°C for 30 minutes. To
415 measure competitive binding of wild type and engineered receptors, cells were instead incubated with 25
416 nM sACE2₂(WT)-IgG1 and 20 nM sACE2₂.v2.4-8h for 30 minutes at 4°C, washed twice, and stained
417 with anti-human IgG-APC (clone HP6017, 1/250 dilution; BioLegend) and anti-HIS-FITC (chicken
418 polyclonal, 1/100 dilution; Immunology Consultants Laboratory) secondary antibodies for 20 minutes at
419 4°C. Finally, in titration experiments, transfected cells were incubated for 30 minutes at 4°C with 1/3
420 serial dilutions of sACE2₂(WT)-8h or sACE2₂.v2.4-8h, followed by two washes and a 30 minute
421 incubation with anti-myc Alexa 647 (clone 9B11, 1/250 dilution) and anti-HIS-FITC (chicken polyclonal,
422 1/100 dilution). For all experiments, cells were washed twice prior to analysis on an Accuri C6 Flow
423 Cytometer (BD Biosciences) and data were processed with FCS Express (De Novo Software).
424 Quantification of myc-S surface expression is detailed in Figure S4.

425 **Reagent and Data Availability.** Plasmids for RBD protein expression are deposited with Addgene
426 (numbers 145145 and 161821-161826). Illumina sequencing data are deposited in NCBI's Gene
427 Expression Omnibus (GEO) under series accession number GSE159372.

428 ACKNOWLEDGEMENTS

429 The Roy J. Carver Biotechnology Center at the University of Illinois assisted with flow cytometry and
430 Illumina sequencing. E.P. designed the study and completed deep mutagenesis. K.K.C. purified proteins,
431 tested BLI kinetics. K.K.C., K.K.N. and T.J.C.T. prepared samples for flow cytometry. This work was in
432 part supported by NIH award R01AI129719 to E.P. The University of Illinois has filed a provisional
433 patent for engineered decoy receptors and E.P. and K.K.C. are co-founders of Orthogonal Biologics, Inc.

434 REFERENCES

- 435 1. P. Zhou *et al.*, A pneumonia outbreak associated with a new coronavirus of probable bat origin.
436 *Nature*. **579**, 270–273 (2020).
- 437 2. A. C. Walls *et al.*, Structure, Function, and Antigenicity of the SARS-CoV-2 Spike Glycoprotein.
438 *Cell* (2020), doi:10.1016/j.cell.2020.02.058.
- 439 3. Y. Wan, J. Shang, R. Graham, R. S. Baric, F. Li, Receptor recognition by novel coronavirus from
440 Wuhan: An analysis based on decade-long structural studies of SARS. *J. Virol.* (2020),
441 doi:10.1128/JVI.00127-20.
- 442 4. D. Wrapp *et al.*, Cryo-EM structure of the 2019-nCoV spike in the prefusion conformation.
443 *Science*, eabb2507 (2020).
- 444 5. M. Hoffmann *et al.*, SARS-CoV-2 Cell Entry Depends on ACE2 and TMPRSS2 and Is Blocked
445 by a Clinically Proven Protease Inhibitor. *Cell* (2020), doi:10.1016/j.cell.2020.02.052.

- 446 6. W. Li *et al.*, Angiotensin-converting enzyme 2 is a functional receptor for the SARS coronavirus.
447 *Nature*. **426**, 450–454 (2003).
- 448 7. M. Letko, A. Marzi, V. Munster, Functional assessment of cell entry and receptor usage for
449 SARS-CoV-2 and other lineage B betacoronaviruses. *Nat Microbiol*. **11**, 1860 (2020).
- 450 8. L. Samavati, B. D. Uhal, ACE2, Much More Than Just a Receptor for SARS-COV-2. *Front. Cell.*
451 *Infect. Microbiol*. **10**, 752 (2020).
- 452 9. F. Jiang *et al.*, Angiotensin-converting enzyme 2 and angiotensin 1–7: novel therapeutic targets.
453 *Nature Reviews Cardiology*. **11**, 413–426 (2014).
- 454 10. L. Zhang *et al.*, The D614G mutation in the SARS-CoV-2 spike protein reduces S1 shedding and
455 increases infectivity. *bioRxiv*, 2020.06.12.148726 (2020).
- 456 11. B. Korber *et al.*, Tracking Changes in SARS-CoV-2 Spike: Evidence that D614G Increases
457 Infectivity of the COVID-19 Virus. *Cell*. **182**, 812–827.e19 (2020).
- 458 12. V. Borges *et al.*, On the track of the D839Y mutation in the SARS-CoV-2 Spike fusion peptide:
459 emergence and geotemporal spread of a highly prevalent variant in Portugal. *medRxiv*,
460 2020.08.10.20171884 (2020).
- 461 13. K. Pyrc *et al.*, Mosaic structure of human coronavirus NL63, one thousand years of evolution. *J.*
462 *Mol. Biol*. **364**, 964–973 (2006).
- 463 14. K. Wu, W. Li, G. Peng, F. Li, Crystal structure of NL63 respiratory coronavirus receptor-binding
464 domain complexed with its human receptor. *Proc. Natl. Acad. Sci. U.S.A.* **106**, 19970–19974
465 (2009).
- 466 15. S. Su *et al.*, Epidemiology, Genetic Recombination, and Pathogenesis of Coronaviruses. *Trends*
467 *Microbiol*. **24**, 490–502 (2016).
- 468 16. M. F. Boni *et al.*, Evolutionary origins of the SARS-CoV-2 sarbecovirus lineage responsible for
469 the COVID-19 pandemic. *Nat Microbiol* (2020).
- 470 17. J. S. M. Sabir *et al.*, Co-circulation of three camel coronavirus species and recombination of
471 MERS-CoVs in Saudi Arabia. *Science*. **351**, 81–84 (2016).
- 472 18. A. Baum *et al.*, Antibody cocktail to SARS-CoV-2 spike protein prevents rapid mutational escape
473 seen with individual antibodies. *Science*, eabd0831 (2020).
- 474 19. A. J. Greaney *et al.*, Complete mapping of mutations to the SARS-CoV-2 spike receptor-binding
475 domain that escape antibody recognition. *bioRxiv*, 2020.09.10.292078 (2020).
- 476 20. M. A. Tortorici *et al.*, Ultrapotent human antibodies protect against SARS-CoV-2 challenge via
477 multiple mechanisms. *Science*, eabe3354 (2020).
- 478 21. D. Pinto *et al.*, Cross-neutralization of SARS-CoV-2 by a human monoclonal SARS-CoV
479 antibody. *Nature* (2020), doi:10.1038/s41586-020-2349-y.
- 480 22. H. Hofmann *et al.*, Susceptibility to SARS coronavirus S protein-driven infection correlates with
481 expression of angiotensin converting enzyme 2 and infection can be blocked by soluble receptor.

- 482 *Biochem. Biophys. Res. Commun.* **319**, 1216–1221 (2004).
- 483 23. C. Lei *et al.*, Neutralization of SARS-CoV-2 spike pseudotyped virus by recombinant ACE2-Ig.
484 *Nat Commun.* **11**, 2070 (2020).
- 485 24. V. Monteil *et al.*, Inhibition of SARS-CoV-2 Infections in Engineered Human Tissues Using
486 Clinical-Grade Soluble Human ACE2. *Cell* (2020), doi:10.1016/j.cell.2020.04.004.
- 487 25. K. K. Chan *et al.*, Engineering human ACE2 to optimize binding to the spike protein of SARS
488 coronavirus 2. *Science*. **4**, eabc0870 (2020).
- 489 26. A. Glasgow *et al.*, Engineered ACE2 receptor traps potently neutralize SARS-CoV-2. *bioRxiv*,
490 2020.07.31.231746 (2020).
- 491 27. Y. Higuchi *et al.*, High affinity modified ACE2 receptors prevent SARS-CoV-2 infection. *bioRxiv*,
492 2020.09.16.299891 (2020).
- 493 28. H. K. Frank, D. Enard, S. D. Boyd, Exceptional diversity and selection pressure on SARS-CoV
494 and SARS-CoV-2 host receptor in bats compared to other mammals. *bioRxiv*. **5**, 562 (2020).
- 495 29. J. Shang *et al.*, Structural basis of receptor recognition by SARS-CoV-2. *Nature*. **382**, 1199
496 (2020).
- 497 30. R. N. Kirchdoerfer *et al.*, Stabilized coronavirus spikes are resistant to conformational changes
498 induced by receptor recognition or proteolysis. *Sci Rep*. **8**, 15701 (2018).
- 499 31. W. Li *et al.*, Receptor and viral determinants of SARS-coronavirus adaptation to human ACE2.
500 *EMBO J.* **24**, 1634–1643 (2005).
- 501 32. D. M. Fowler, S. Fields, Deep mutational scanning: a new style of protein science. *Nat. Methods*.
502 **11**, 801–807 (2014).
- 503 33. J. D. Heredia *et al.*, Mapping Interaction Sites on Human Chemokine Receptors by Deep
504 Mutational Scanning. *J. Immunol.* **200**, ji1800343–3839 (2018).
- 505 34. J. Park *et al.*, Structural architecture of a dimeric class C GPCR based on co-trafficking of sweet
506 taste receptor subunits. *Journal of Biological Chemistry*. **294**, 4759–4774 (2019).
- 507 35. D. M. Fowler, C. L. Araya, W. Gerard, S. Fields, Enrich: software for analysis of protein function
508 by enrichment and depletion of variants. *Bioinformatics*. **27**, 3430–3431 (2011).
- 509 36. T. N. Starr *et al.*, Deep Mutational Scanning of SARS-CoV-2 Receptor Binding Domain Reveals
510 Constraints on Folding and ACE2 Binding. *Cell*. **182**, 1295–1310.e20 (2020).
- 511 37. T. W. Linsky *et al.*, De novo design of ACE2 protein decoys to neutralize SARS-CoV-2. *bioRxiv*,
512 2020.08.03.231340 (2020).
- 513 38. Y. Cai *et al.*, Distinct conformational states of SARS-CoV-2 spike protein. *Science*. **369**, 1586
514 (2020).
- 515 39. H. Yao *et al.*, Molecular architecture of the SARS-CoV-2 virus. *Cell* (2020).

- 516 40. G. J. Rocklin *et al.*, Global analysis of protein folding using massively parallel design, synthesis,
517 and testing. *Science*. **357**, 168–175 (2017).
- 518 41. L. Cao *et al.*, De novo design of picomolar SARS-CoV-2 miniprotein inhibitors. *Science*,
519 eabd9909 (2020).
- 520 42. S. S. Usmani *et al.*, THPdb: Database of FDA-approved peptide and protein therapeutics. *PLoS*
521 *ONE*. **12**, e0181748 (2017).
- 522 43. J. Park *et al.*, Engineered receptors for human cytomegalovirus that are orthogonal to normal
523 human biology. *PLoS Pathog*. **16**, e1008647 (2020).
- 524 44. Y. Imai *et al.*, Angiotensin-converting enzyme 2 protects from severe acute lung failure. *Nature*.
525 **436**, 112–116 (2005).
- 526 45. B. Trembl *et al.*, Recombinant angiotensin-converting enzyme 2 improves pulmonary blood flow
527 and oxygenation in lipopolysaccharide-induced lung injury in piglets. *Crit. Care Med*. **38**, 596–
528 601 (2010).
- 529 46. P. Verdecchia, C. Cavallini, A. Spanevello, F. Angeli, The pivotal link between ACE2 deficiency
530 and SARS-CoV-2 infection. *Eur J Intern Med*. **76**, 14–20 (2020).
- 531 47. D. Wang *et al.*, Renin-angiotensin-system, a potential pharmacological candidate, in acute
532 respiratory distress syndrome during mechanical ventilation. *Pulm Pharmacol Ther*. **58**, 101833
533 (2019).
- 534 48. M. K. Chung *et al.*, SARS-CoV-2 and ACE2: The biology and clinical data settling the ARB and
535 ACEI controversy. *EBioMedicine*. **58**, 102907–102907 (2020).
- 536 49. J. A. Johnson, J. West, K. B. Maynard, A. R. Hemnes, ACE2 improves right ventricular function
537 in a pressure overload model. *PLoS ONE*. **6**, e20828 (2011).
- 538 50. P. Liu *et al.*, Novel ACE2-Fc chimeric fusion provides long-lasting hypertension control and
539 organ protection in mouse models of systemic renin angiotensin system activation. *Kidney Int*. **94**,
540 114–125 (2018).
- 541 51. M. Haschke *et al.*, Pharmacokinetics and pharmacodynamics of recombinant human angiotensin-
542 converting enzyme 2 in healthy human subjects. *Clin Pharmacokinet*. **52**, 783–792 (2013).
- 543 52. A. Khan *et al.*, A pilot clinical trial of recombinant human angiotensin-converting enzyme 2 in
544 acute respiratory distress syndrome. *Crit Care*. **21**, 234 (2017).
- 545 53. N. Iwanaga *et al.*, Novel ACE2-IgG1 fusions with improved activity against SARS-CoV2.
546 *bioRxiv*, 2020.06.15.152157 (2020).
- 547 54. E. Procko *et al.*, Computational design of a protein-based enzyme inhibitor. *J. Mol. Biol*. **425**,
548 3563–3575 (2013).

549